Journal Pre-proof

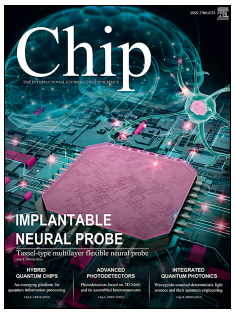

Machine Learning-Accelerated Discovery of Novel 2D Ferromagnetic Materials with Strong Magnetization

Chao Xin, Yaohui Yin, Bingqian Song, Zhen Fan, Yongli Song, Feng Pan

PII: S2709-4723(23)00034-5

DOI: https://doi.org/10.1016/j.chip.2023.100071

Reference: CHIP 100071

To appear in: *Chip*

Received Date: 7 July 2023

Revised Date: 20 August 2023

Accepted Date: 10 October 2023

Please cite this article as: Xin C, Yin Y, Song B, Fan Z, Song Y, Pan F, Machine Learning-Accelerated Discovery of Novel 2D Ferromagnetic Materials with Strong Magnetization, *Chip*, https://doi.org/10.1016/j.chip.2023.100071.

Adaptive machine learning for predicting the magnetism of two-dimensional materials.

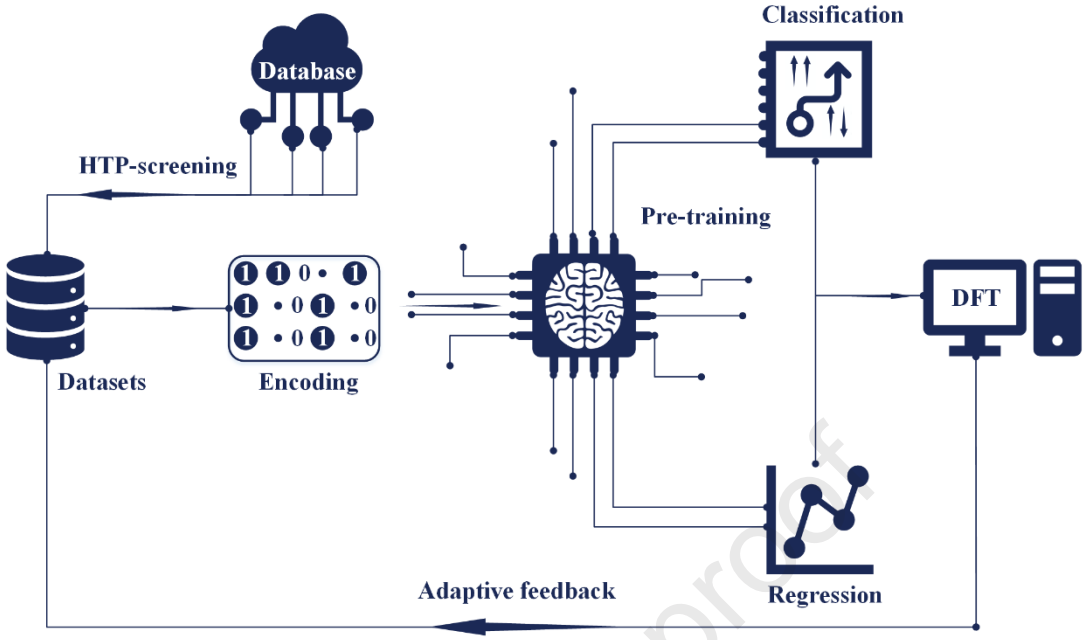

MATERIALS DOI:10.1016/j.chip.20xx.1000xx

Machine Learning-Accelerated Discovery of Novel 2D Ferromagnetic Materials with Strong Magnetization

Chao Xin[1,2,*], Yaohui Yin[1], Bingqian Song[3], Zhen Fan[1], Yongli Song[4,*] and Feng Pan[2,*]

[1] School of Science, Changchun University of Science and Technology, Jilin Key Laboratory of Solid-State Laser Technology and Application, Changchun 130022, China

[2] School of Advanced Materials, Peking University Shenzhen Graduate School, Shenzhen 518055, China

[3] Center for Lattice Defectronics & Department of Physics, KAIST, Daejeon 34141, Republic of Korea

[4] School of Energy and Power Engineering, JiangSu University, Zhenjiang 212013, China

*Corresponding author. E-mail addresses:
E-mails: chaoxin@pkusz.edu.cn (C. Xin), songyl@ujs.edu.cn (Y. L. Song), panfeng@pkusz.edu.cn (F. Pan)

ABSTRACT

Two-dimensional ferromagnetic (2DFM) semiconductors (metals, half-metals, and so on) are important materials for next-generation nano-electronic and nano-spintronic devices. However, these kinds of materials remain scarce, and "trial and error" experiments and calculations are time-consuming and expensive. In the present work, to obtain optimal 2DFM materials with strong magnetization, we established a machine learning (ML) framework to search the 2D material space containing over 2417 samples, and identified 615 compounds whose magnetic orders was then determined via high-through-put first-principles calculations. Using ML algorithms, we trained two classification models and a regression model. The interpretability of the regression model was evaluated through Shapley additive explanations (SHAP) analysis. Unexpectedly, we found that Cr_2NF_2 is a potential antiferromagnetic ferroelectric 2D multiferroic material. More importantly, 60 novel 2DFM candidates were predicted, and among them, 13 candidates have magnetic moments of > 7 μ_B. Os_2Cl_8, Fe_3GeSe_2, and $Mn_4N_3S_2$ were predicted to be novel 2DFM semiconductors, metals, and half-metals, respectively. Our ML approach can accelerate the prediction of 2DFM materials with strong magnetization and reduce the computation time by more than one order of magnitude.

Keywords: 2D ferromagnetic; machine learning; high through-put screening; DFT; model interpretability

INTRODUCTION

Two-dimensional ferromagnetic (2DFM) materials have several unique properties that make them promising for potential device applications, such as sensing, memory technologies, 2D spintronics and valleytronics.[1–4] According to the Mermin-Wagner theorem, under an isotropic Heisenberg model at finite temperatures, long-range magnetic order must be suppressed because of thermal fluctuations.[5] However, more recent discoveries of 2DFM, for instance, the CrI_3, $Cr_2Ge_2Te_6$, $MnSe_2$, and

MATERIALS DOI:10.1016/j.chip.20xx.1000xx

Fe_3GeTe_2 monolayers have attracted widespread attention.[6-12] Numerous 2D materials have been computationally predicted by using the high throughput density functional theory (DFT),[13] resulting in a few public and open-source 2D materials databases, e.g., Computational 2D Materials Database (C2DB),[14] 2D Materials Encyclopedia (2DMP),[15] Materials Cloud two-dimensional crystals database (MC2D)[16], that consist of hundreds to thousands of samples. Although these databases cover the dynamic and thermodynamic stabilities of 2D materials, as well as electronic structure information, there are two problems in the study of magnetism. First, the materials classification of 2DFM in the database is not accurate enough; all possible antiferromagnetic (AFM) orderings were not considered to accurately determine the actual magnetic ground state, and the calculation magnetic moments is still imprecise. Second, only few 2DFM candidates have been experimentally synthesized thus far, and the magnetizations of these 2DFM materials are fairly weak. This indicates that the information on magnetism in the database does not provide accurate guidance for obtaining excellent 2DFM materials in experiments. Trial-and-error experiments and calculations are time-consuming and expensive.

Machine-learning (ML) algorithm are a more rapid and efficient method for 2DFM material discovery, and provide many new candidates with excellent properties for experiments. In contrast to traditional first principles calculations based on DFT that need to solve the many-body Kohn-Sham equation, ML approaches are Big Data driven, and can map the given material features to desired properties.[17] ML has inherent advantages for efficient searching target properties among enormous material spaces. This novel scientific paradigm[18] has been successfully applied to the prediction of various functional materials, such as lithium batteries,[19] photovoltaic materials,[20] catalysts.[21] Despite the advantages of ML algorithm for 2D functional materials, they have rare applications in 2D magnetic systems, mainly owing to the lack of suitable feature descriptors for 2D magnetic material systems. Descriptors based on several feature vectors from elemental properties and compositions exhibit excellent performance in property prediction, but do not work well on a small dataset, including samples with various crystal structures. Many common descriptors, such as property-labelled materials fragments (PLMF),[22] materials graph networks,[23] and crystal graph convolutional neural networks[24] show excellent performance for various structures, but require large datasets. Furthermore, most of these features lack important information on the magnetic and electronic properties, such as unpaired *d* orbital electrons.[25]

ML algorithms have been used to investigate magnetic properties in a few published studies. Through the on-the-fly interpretable ML, 2DFMs with high Curie temperatures were discovered by Wang et al.[26] Acosta et al. proposed an ML-based strategy to analyze and predict magnetic ordering in 2D materials.[27] Kabiraj et al. developed a fully automated, graphics processing unit (GPU)-accelerated, end-to-end ML model to the 2DFM materials with high Curie points.[28] An adaptive

framework to accelerate the discovery of 2D intrinsic ferromagnetic (FM) materials was developed, in which ML is combined with high-throughput DFT calculations.[29] A ML-assisted hierarchical screening strategy for predicting magnets with high stability and large anisotropy energy was proposed by Sen et al.[30] Nonetheless, it remains a tremendous challenge for ML approaches to accurately predict the magnetic and electronic properties of 2D materials.

In the present work, we present a data-driven ML strategy to study the magnetism in 2D materials. In contrast to traditional DFT calculations, we focus on exploring the material property relationship to establish the simplest correlation between the magnetic structure and features, such as crystal structure, composition, and elemental properties. We trained three ML models using DFT calculations and a recently updated database of 2D materials to obtain features capable of classifying 2D materials as NM, FM, or AFM and predicting 2DFMs with strong magnetization. Our strategy mainly includes three aspects: (i) we first develop an ML model to distinguish magnetic candidates from nonmagnetic candidates according to the composition and elemental properties, and build a model to classify the FM and AFM materials in a high-throughput DFT-calculated dataset; (ii) on the basis of the unpaired *d* orbital electrons of the transition metal (TM) and features strongly related to the structure, we establish an ML regression model to predict the net magnetic moment of 2DFMs unit cell; and (iii) using the established ML model, we expedite the discovery of novel 2D magnetic materials with strong magnetization.

RESULTS AND DISCUSSION

ML computational framework

We first describe the workflow of our ML code, as shown in Fig. 1. We extracted stable 1617 samples from the C2DB dataset, of which 1292 samples were labeled as nonmagnetic 2D materials and 325 were labeled as magnetic. This imbalanced dataset could not be used to train the classification models. Therefore, 800 2D magnetic materials were randomly selected from the 2DMP database. The new dataset included 2417 samples that were used to pre-train the classification model for magnetic/nonmagnetic 2D materials. After we obtained model-N-M, the 615 samples with magnetic moments of $> 1\ \mu_B$ were fed to high-throughput calculation to train the FM-AFM classification model. In this step, we obtained an FM/AFM classification model and a dataset of 2D materials with precise magnetic moments. In the next step, we discarded the AFM 2D materials and trained a regression model of magnetization (model-R). We selected 545 stable magnetic samples from the recently updated C2DB and removed duplicate samples from the previous database. We use non-prior samples as a validation set to predict new materials. Finally, we selected 2D materials with magnetic moments of $> 7\ \mu_B$ and defined them as strongly magnetized materials. Our hierarchical filtering process does not depend on empirical parameters or physical intuition, and the database is updated in real time. Finally, we analyzed the interpretability of the model. Our ML predictions and DFT calculations

did not target the Curie point, because Kabiraj et al. have already calculated this through GPU acceleration.[28] Additionally, the C2DB database does not contain the Curie point, and no experimental values have been reported for the magnetic transition critical temperatures of most 2D materials.

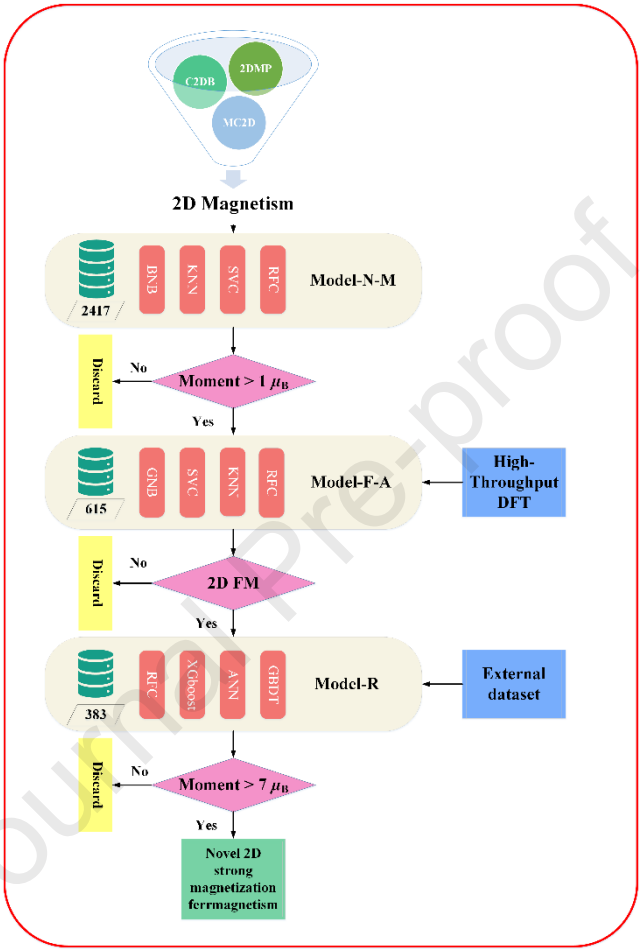

Fig. 1 | Workflow for hierarchical screening of 2D materials for classification of magnetic-nonmagnetic, FM/AFM classification and prediction of net magnetic moment followed by confirmation in DFT. Achieving a two-dimensional material design with strong magnetization ultimately.

Classification model for magnetic/nonmagnetic and FM/AFM materials

Our ultimate-goal was to develop novel 2DFM materials with strong magnetization. Therefore, a two-step ML model was constructed. The first step of ML was to classify 2D materials into magnetic and nonmagnetic groups according to their class labels of magnetic states in the C2DB and 2DMP databases, and *data-M-N* was adopted for this task. Model-M-N performs binary classification to distinguish magnetic and nonmagnetic 2D materials from the dataset *data-M-N*. We selected the following four algorithms to train this binary model: Bernoulli Naive Bayes (BNB), K-Nearest Neighbor (KNN), Support Vector Machine Classifier (SVC), Random Forest Classifier (RFC). All the ML algorithms used in the present work were

implemented through the Scikit-learn library (version 1.1.3).[44] Because the dataset used in our first model was of medium size, the training and test sets were randomly split at a 7:3 ratio. The ML models were trained using 2D material data in the training set, and the generalization ability and accuracy of the ML model were tested using 2D material data in the test set. A 10-fold cross-validation approach was used for optimize the hyperparameters in all the models. The performance metrics of the test set for all four models are presented in Table 1. As shown, KNN and BNB had similar metrics. SVC with the rbf kernel performed better than KNN and BNB. The RFC classifier achieved the best performance for all the metrics. The receiver operating characteristic (ROC) curves and typical confusion matrices for the four classification tasks are shown in Fig. 2. The optimized hyperparameters for all the models are presented in Table S2, and the Supplemental Information (SI) details the classification techniques utilized. The classification area under the curve (AUC) value of the RFC model for the non-magnetic/magnetic classifications exceeded 90% after re-examination of distinguishable samples. The confusion matrix for each classifier presents the counts of the classes predicted using the four algorithms versus the true classes of the test set. Excellent performance was achieved particularly for RFC classification, with an AUC value of 0.94.

Table 1 | Test-set performance metrics of ML models for classification of materials as magnetic/nonmagnetic.

Model	Accuracy	Precision	Recall	F1
BNB	0.758	0.745	0.728	0.737
KNN	0.780	0.770	0.752	0.760
SVC	0.851	0.832	0.852	0.842
RFC	0.877	0.867	0.870	0.869

To further verify the generalizability of the model, we constructed a dataset containing 10 2D materials: CrI_3, $CrGeTe_3$, $PrTe_3$, $TiPb_9O_{11}$, TaSe, $InCl_3$, $TiGeTe_6$, $KB(CO_2)_4$, Ag_2WS_4, and NaFeAs. In this small validation set, CrI_3 and $CrGeTe_3$ are known 2D magnetic materials, and the other eight materials are labeled as nonmagnetic materials and are taken from 2DEP. The test results are presented in the Table S3, where the Boolean values “True/False” represent magnetic and nonmagnetic materials, respectively. The four algorithms accurately classified CrI_3 and $CrGeTe_3$ as magnetic materials.[45] However, the most accurate classification model remained the RFC algorithm. Once again, our goal was to predict strongly magnetized ferromagnetic materials. Therefore, at this stage, we did not perform DFT calculations to determine whether materials that have not been reported have magnetism.

MATERIALS

DOI:10.1016/j.chip.20xx.1000xx

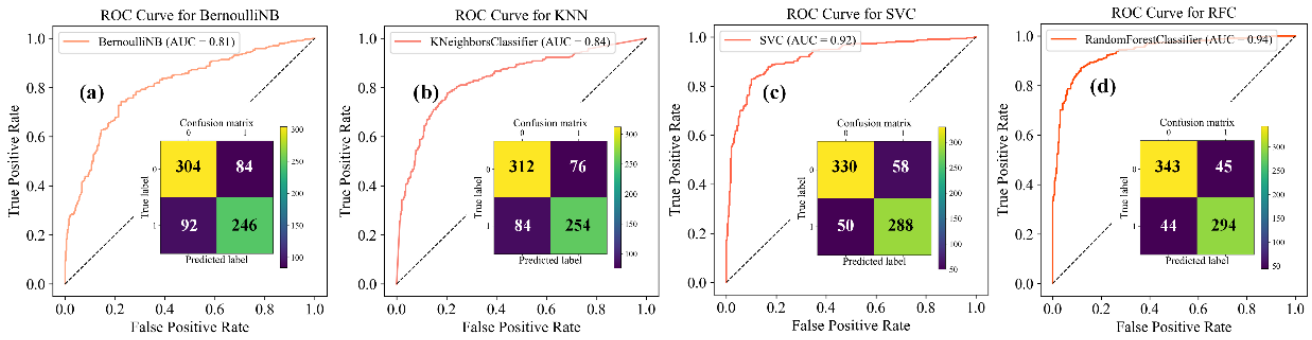

Fig. 2 | Test performance of machine learning classification model for magnetic-nonmagnetic with four classified algorithms (a) BernoulliNB, (b) KNN, (c) SVC, (d) RFC. Insert: typical confusion matrices for the magnetic/nonmagnetic binary classification tasks.

In the second step, the FM/AFM classification of the selected magnetic candidates are performed using model-F-A with four ML algorithms. The second step included two sub-steps: high-throughput DFT calculation and FM/AFM classification. After simple screening of the old C2DB database, 615 samples have thermodynamic and dynamic stability, and along with magnetic moments > 1 μ_B. However, as mentioned previously, the 615 samples were all labeled as FM. The calculation results in the C2DB database were based on a unit cell, and most of them were obtained using GGA or HSE approximations. This resulted in all materials being incorrectly calculated as ferromagnetic, whereas the antiferromagnetic materials were completely ignored. In addition, for magnetic systems, the GGA may underestimate the band gap and magnetic moment of 2D strong-correlation materials.[46] To obtain an accurately labeled dataset of FM/AFM, we re-calculated the 615 2D candidates using the GGA+*U* approach. The detailed Hubbard *U* values of the TM are presented in Table S1, where only the one on element Tc is null. A 2 × 1 × 1 super-cell was built for the unit cell, which included only one magnetic atom. In our calculations, AFM represented the spin-antiparallel arrangement of two magnetic atoms, and more complex magnetic structures were not considered. Structural relaxation was performed on all materials, and the free energies of FM and AFM materials were calculated. The energy differences between the FM and AFM are presented in Table S4. The calculation results indicated that 357 materials are ferromagnetic, 223 are antiferromagnetic, 26 have ferromagnetic energy equal to the antiferromagnetic energy, and nine materials are quinary compounds that were discarded in our ML model. 26 materials with equal ferromagnetic and antiferromagnetic energies were divided into antiferromagnetic sets. Therefore, the ratio of the number of samples in the FM and AFM sets was 1.43:1. We further classified the 2DFM materials into diverse prototypes according to their structural symmetries and space groups. Among the 357 2DFM materials, the 10 most common ones, representing all 300 structures, are shown in Fig. 3. The most common space group was that of *P*-3*m*1, which corresponded to 77 similar structures, including

many MXenes and TM dichalcogenides. We found that most 2DFM materials have not been reported, and their structural prototypes are novel and compelling.[47] Moreover, we emphasize that the Hf_2Br_6 with *P*-62*m* space group and Os_2Cl_6 with *P*6/*mmm* space group both have a TM in the sixth period; they have not been reported before and are rare in 2D ferromagnetism.

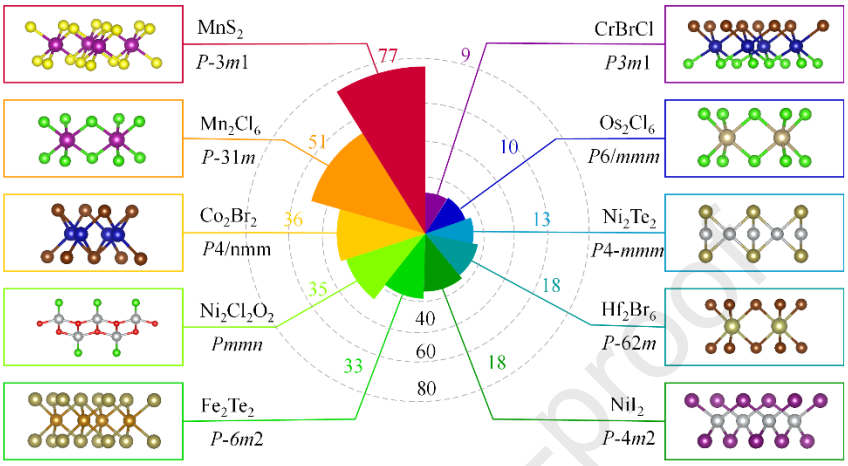

Fig. 3 | The most common 2D ferromagnetic structural prototypes. Polar radar graph illustrating the number of structures corresponding to the ten most common 2D ferromagnetic structural prototypes in the set of 383 2D systems of accurate DFT calculation. A histogram representation of each structural prototype is shown, together with the structure-type space group and the formula of the 2D ferromagnetic materials.

After high-throughput DFT calculations, the 606 samples obtained were used to train the FM and AFM classification model-F-A. Because this dataset was small and the performance of the generalization ability of training sets on test sets may be affected by a particular random training-test set split, the train and test set were randomly split at an 8:2 ratio. Hyperparameter optimization for the models involved a 10-fold cross-validation technique. The main metrics for the FM/AFM classification of the test set are presented in Table 2. The KNN and RFC classifiers performed significantly better than the SVC and GNB classifiers. To increase the classification accuracy of the Naive Bayesian algorithm, we replaced the Bernoulli Naive Bayesian with the Gaussian Naive Bayesian; however, the accuracy did not increase. Again, the RFC classifier achieved an excellent test-set accuracy of 0.918. For the magnetic/nonmagnetic classification models, the four metrics were relatively averaged. However, for the FM/AFM classifier, the precision was higher than the accuracy, and the recall was lower than the precision for the KNN and RFC classifiers. The ROC curves and typical confusion matrices for the four classification tasks are shown in Fig. 4. The optimized hyperparameters for all the models are presented in Table S5. The classification AUC value of the RFC model for the FM/AFM classifications exceeded 95% after re-examination of distinguishable samples. The confusion matrix for each classifier presents the counts of the classes predicted using the four algorithms versus the true classes of the test set. Excellent performance was achieved, especially for RFC classification, with an AUC value has reached 0.97.

MATERIALS DOI:10.1016/j.chip.20xx.1000xx

Table 2 | Test-set performance metrics of ML models for classification of materials as FM/AFM.

Model	Accuracy	Precision	Recall	F1
GNB	0.779	0.759	0. 917	0.830
SVC	0.869	0.938	0.833	0.882
KNN	0.902	0.929	0.903	0.916
RFC	0.918	0.943	0.917	0.930

To verify the generalization ability of model-F-A and quickly predict new ferromagnetic materials, we selected 542 samples labeled as magnetic in the updated C2DB database and screened them to obtain 463 2D materials with a magnetic moment of > 1 μ_B. Compared with previous dataset of 615 samples, duplicate compounds and quinary compounds were removed, resulting in 167 candidates. This small dataset was used as a validation set and imported into the RFC model-F-A for classification. We predicted that 60 of these compounds are ferromagnetic, as shown in Table S6.

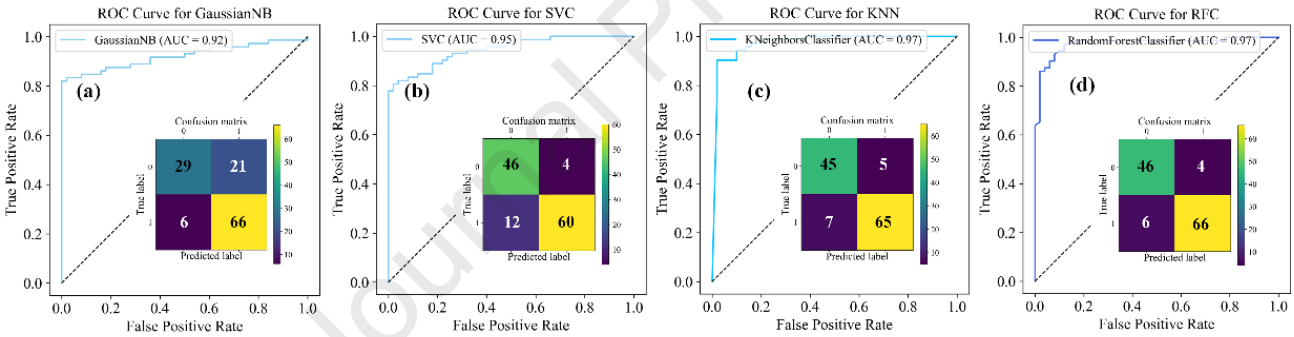

Fig. 4 | Test performance of machine learning classification model for FM/AFM with four classified algorithms (a) GaussianNB, (b) SVC, (c) KNN, (d) RFC. Insert: typical confusion matrices for the FM/AFM binary classification tasks.

Feature selection is critical for ML models. Fig. 5 shows the sorting results for the material features of the RFC model. As indicated by Fig. 5(a), the following were among the top 10 features in the dataset examined: (i) the electronegativity, covalent radius, Mendeleev number, and melting ("mode electronegativity", "mean electronegativity", "CovalentRadius", "Minimum MendeleevN", "Range MeltingT", and "Maximum MeltingT"), which are correlated to the elemental properties; (ii) the number of the space group (SGnumber), which is linked to the structural symmetry; and (iii) GSvolume_pa, NpUnfilled and NUnfilled, which affect the contributions of different elements in the materials to the top of the valence band, thus affecting the electronic band structure and magnetic properties of the compounds. As shown in Fig. 5(a), even without considering structural features as descriptors, we can obtain a magnetic/nonmagnetic classification model (model-M-N) with high generalization ability and scores using only element and component features. However, after testing, the same set of features

was used to train the AFM/FM classification models, which resulted in extremely low scores for each metric. This originates from the feature vector of a single TM element cannot determine the magnetic order of the system, and both ferromagnetic and antiferromagnetic interactions are associated with the exchange interactions of the adjacent magnetic atoms. The types of TM ions, the corresponding ligand atoms, and their ionic radii lead to the formation of different types of crystal fields in the compounds. As reported by Wang et al. the crystal fields are an important feature used to describe magnetic ordering[26] particularly the ability to classify FM and AFM materials. Therefore, during the training of model-F-A, we introduced the properties of the ligand atoms as feature vectors. We also introduced structural features, as well as 20 atom centered symmetry function (ACSF) features associated with structures. Fig. 5(b) shows the sorting results for the material features of the RFC model-F-A. All the elemental features and their descriptions (spin magnetic moments, ionic radius, covalent radius, dipole polarization, formation heat, electronegativity, and vdw radius) were obtained from the Python Mendeleev package 0.11.0.[34] We performed a simple summation process on the elemental features of TM atoms and their coordinate atoms, and we added the *d* orbital electron number of the TM to the feature sets. As shown in Fig. 5(b), the sum of the ionic radii of the TM and coordination atoms and the ionic radii of the coordinate atoms were the most important features. In contrast, the ACSF did not have a significant impact on the nature of the target materials.

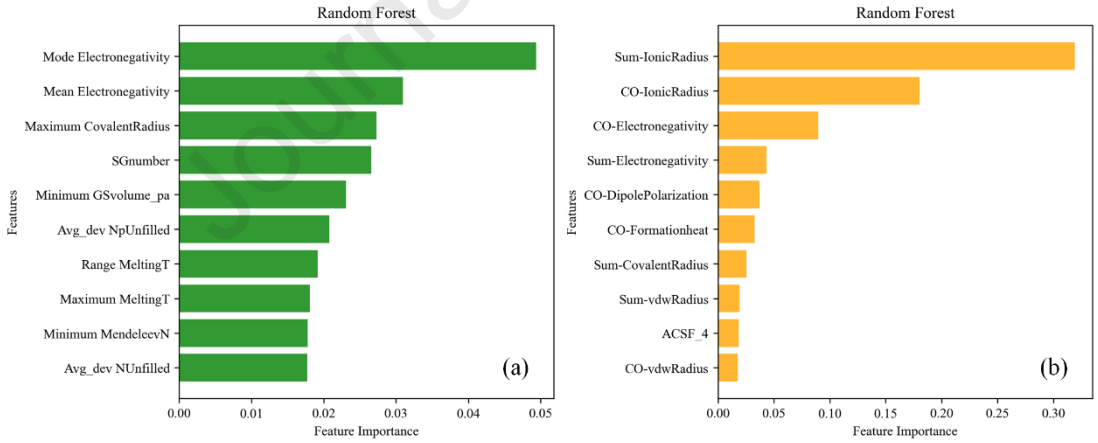

Fig. 5 | Importance of different groups of features in different tasks in the RFC classifier. (a) model-M-N, (b) model-F-A. See supporting information for details.

According to our high-throughput calculations, most 2D magnetic materials have not been reported, and a special one is Cr_2NF_2, which has a negative energy difference between FM and AFM states, indicating that the ferromagnetism is stable. However, according to our recent work, Mo_2NCl_2 is a zigzag-type AFM.[48,49] This is because in our high-throughput calculations, the FM and Néel AFM orders were simply considered, whereas the ground state magnetic structure of this functionalized MXene material is a zigzag type AFM state. Therefore, we selected three magnetic structures, as shown in Fig. S1, found that Cr_2NF_2

MATERIALS DOI:10.1016/j.chip.20xx.1000xx

is a potential antiferromagnetic/ferroelectric multiferroic material. To estimate the Nèel temperature (T_N) of the ferrimagnetic Cr_2NF_2, Monte Carlo (MC) simulations based on the 2D Heisenberg Hamiltonian model were performed. Details regarding the MC simulations are provided in the SI. From the calculated curve of C_v, as shown in Fig. 6(a), we found that Cr_2NF_2 had a fairly high T_N of 169 K. The non zero magnetic moment at 0 K reflects the antiferromagnetic behavior of the ground state, as shown in Fig. 6(b). Cr_2NF_2 has a higher magnetic transition temperature than CrI_3 (T_C = 45 K) and $Cr_2Ge_2Te_6$ (T_C = 30 K),[50,51] suggesting its potential applications in nano-spintronic devices. In addition, the ferroelectric polarization switching process was also simulated using the NEB approach, as shown in Fig. 6(c). As the paraelectric state is dynamically unstable, the energy profile is a double-well curve. Two degenerate polarized states pass through a saddle point (0.276 eV).

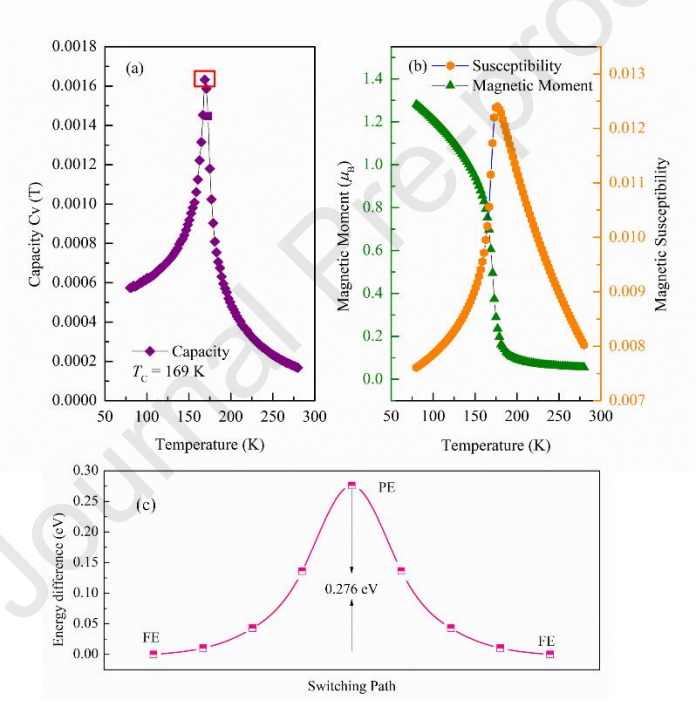

Fig. 6 | The results of Monte Carlo simulations (a) Specific heat Cv as a function of temperature, (b) Magnetic moment and magnetic susceptibility as functions of temperature for Cr_2NF_2. (c) The energy barrier of possible ferroelectric switching path for Cr_2NF_2.

Regression model of net magnetic moments

Most reports on magnetic moment prediction focus on the atomic magnetic moment of each TM,[52] or the magnetic moment per atom.[53] So it is hard to believe that it fully reflects the total magnetization of the system. According to model-F-A and the high-throughput DFT results, there were 383 candidates, including 357 ferromagnetic and 26 energy-degenerate FM/AFM states, which were used to train the regression model of the net magnetic moments of the unit cell. A material information platform (Matminer) was used to describe elemental features of the materials in the dataset.[54] Elemental properties mainly

MATERIALS DOI:10.1016/j.chip.20xx.1000xx

include elemental information, the electronic configuration, and the material composition. In addition, we added 20 sine Coulomb matrix eigenvalues and 116 SOAP features associated with the structure. Thus, 273 features were included in the dataset. The input of high-dimensional features not only leads to risky of overfitting but also models inefficiency. The most important features were evaluated and retained using 10-fold cross-validation recursive feature elimination (RFECV). Through this procedure, 24 features were obtained, which were used for the subsequent model training and testing. In Table S8, 24 selected significant features are shown, and the physical explanation of each feature is presented in Table S8. In addition, the number of unpaired *d* orbital electrons of the TM elements (*N*-*e*-unpaired) and the magnetic moment of a single TM atom calculated using DFT (M-single atom) were important features for training the regression model. Unlike classification models, during the training of regression models, we selected three ensemble algorithms Random Forest Regression (RFR), Gradient Boosting Decision Tree (GBDT), eXtreme Gradient Boosting (XGboost) and an Artificial Neural Network (ANN) algorithm.[55] The selected hyperparameters for the four models are presented in Table S7.

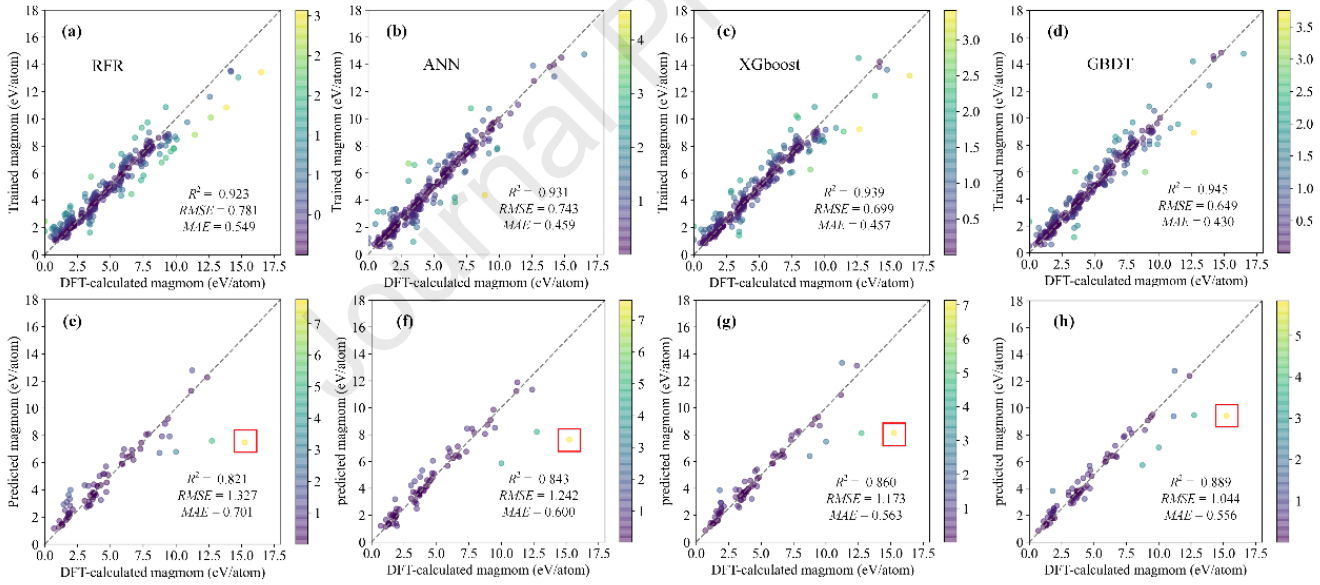

Fig. 7 | The training results of (a) RFR, (b) ANN, (c) XGboost, and (d) GBDT models, and testing results of (e) RFR, (f) ANN, (g) XGboost, and (h) GBDT models. The gray dash line in each figure represents the ideal curve y = x. The color bar represents absolute error. The red rectangular box represents the anomalous point, which is Fe_4S_8.

Fig. 7 shows the results of the training and testing of the net magnetic moment of the unit cell for the four regression models. As indicated by Figs. 7(a)-(d), the training scores of all four models were high, indicating that the 25 features (24 optimized features and *N*-*e*-unpaired) are closely related to the net magnetic moment. The R^2 scores of the three ensemble and ANN models were all > 0.9, and the GBDT model exhibited the best performance, with R^2 = 0.945. It also exhibited the smallest

MATERIALS DOI:10.1016/j.chip.20xx.1000xx

RMSE and *MAE* of 0.649 and 0.430 μ_B, respectively. The test results indicated that all four models have excellent generalization abilities, as shown in Figs. 7(e)-(h). The GBDT model achieved the highest performance among the four ML regression models, with the smallest *MAE* of 0.556 μ_B, exhibiting superior prediction accuracy. The regression models trained using 25 features (24 optimized features and M-single atoms) are shown in Fig. S2. The training accuracy of the model containing *N-e*-unpaired features was similar to that of the model containing M-single atom features. However, M-single atom features require expensive and accurate DFT calculations. Therefore, in our subsequent prediction of 2D materials with strong magnetization, the ML model used was a regression model with *N-e*-unpaired features.

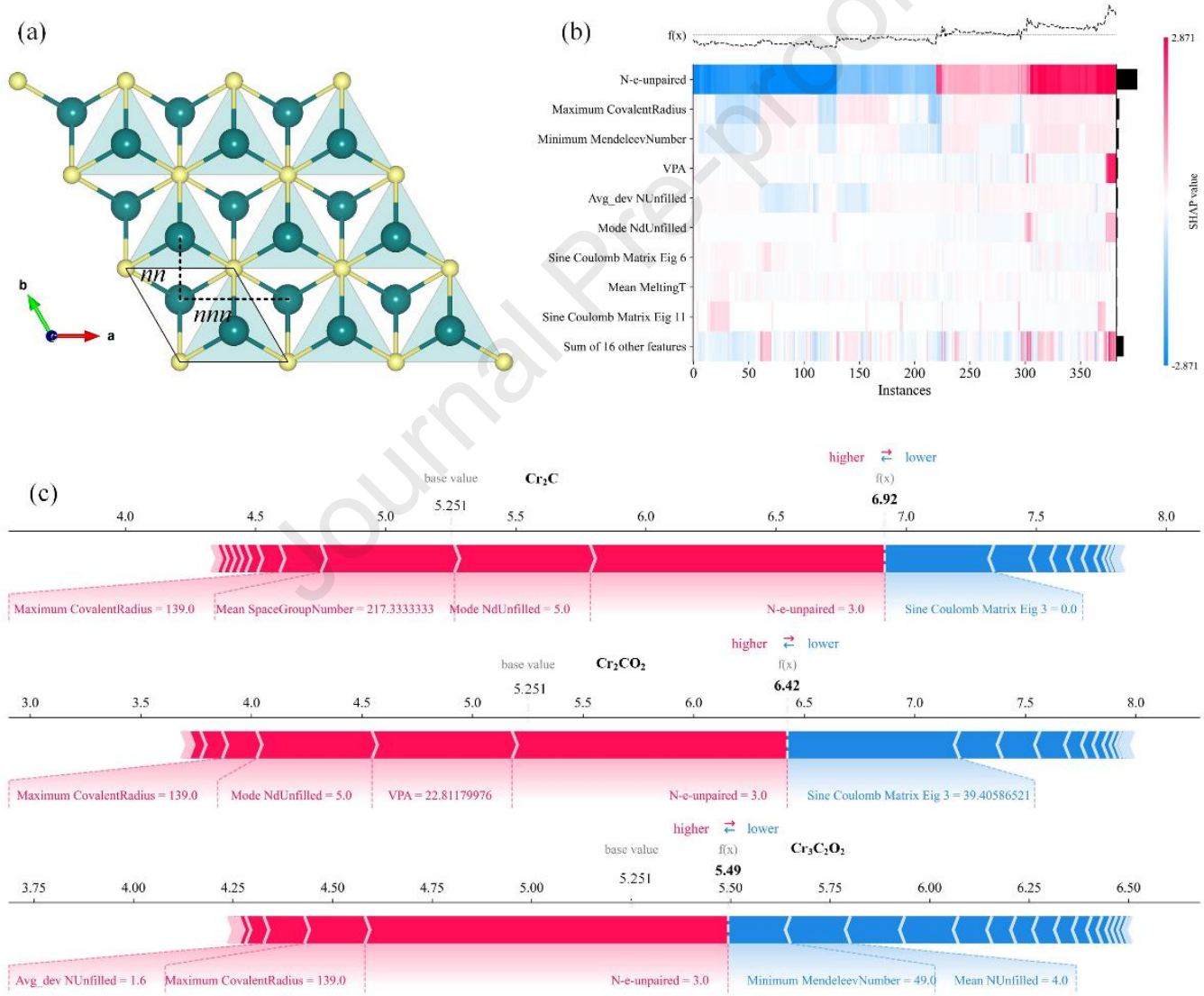

Fig. 8 | (a) monolayer structure of Cr_2C, (b) the heatmap matrix of the SHAP value magnitude of optimized structural and magnetic features; (c) SHAP analysis of Cr_2C, Cr_2CO_2, and $Cr_3C_2O_2$. Positive (red) and negative (blue) SHAP value represents

the contribution of a single sample to the net magnetic moments. The expected base value of magnetic moments is 5.251 μ_B, and the machine learning predicted value is highlighted in black.

SHAP value analysis is an approach for evaluating ML model interpretability. It can provide a clear graph of how diverse features compete with each other and determine the target property.[56] Specifically, it can reveal the quantitative local contribution of each feature to the prediction target property of a single sample, which is difficult to explain by feature importance. Therefore, SHAP value analysis was implemented on the optimized dataset of the magnetic moment regression model. The SHAP values of the 25 most important elemental and magnetic features of the magnetic moment regression model are shown in Fig. 8. The exchange interaction between the nearest-neighbor (nn) and next-nearest-neighbor (nnn) atoms in 2D monolayer materials has a more significant effect on the magnetic moment than the elemental or atomic properties.[57] Taking Cr_2C as example, the crystal field affects the electronic structure, which in turn affects the magnetic interaction of magnetic systems, as shown in Fig. 8(a). The sine Coulomb matrix, volume per atom (VPA), are related to the structural properties, which are also vital for the prediction of net magnetization, as shown in Fig. 8(b). The local influence of the optimal representation set was also analyzed. We selected Cr_2C, Cr_2CO_2, and $Cr_3C_2O_2$ as representative materials, and their SHAP values for the preferred features are shown in Fig. 8(c). The net magnetic moment is 6.92, 6.42, and 5.49 μ_B per supercell for Cr_2C, Cr_2CO_2, and $Cr_3C_2O_2$, respectively. Among the preferred features for enhancing the net magnetic moment, the *N*-*e*-unpaired is the most positive contribution. Conversely, the "sine Coulomb matrix eig 3", and mean number of unfilled electrons are the features with the most negative contributions. The *N*-*e*-unpaired of pristine and O_2 functionalized Cr_2C are similar in contribution. The contribution of *N*-*e*-unpaired increases from two to three layers of TM (Cr_2C to Cr_3C_2). Additionally, the proportion of VPA in Cr_2CO_2 is relatively high, and the maximum covalent radii of Cr_2CO_2 and $Cr_3C_2O_2$ gradually increased. This leads to a shorter distance between the two *nn* Cr^{3+} ions. Thus, the Cr-C-Cr FM super-exchange interaction in monolayer MXenes becomes stronger. Owing to the complexity of 2D structures and the various factors affecting their magnetism, the SHAP value provides only limited information on the physical mechanism. Nevertheless, the SHAP value analysis makes our ML model for predicting 2D materials with strong magnetization more interpretable. Significantly, we employ the SHAP method for a quantitative analysis of the impact of ML-selected features on magnetic properties, thereby revealing the underlying physical insights of our models. This interpretable framework has the potential to unlock the "black box" of ML, which could lead to groundbreaking ML-aided material design advancements.

Design of novel 2D magnetic materials with strong magnetization.

The aim of this section is to design 2D materials with large net magnetic moments for the afore mentioned reasons. Using

MATERIALS DOI:10.1016/j.chip.20xx.1000xx

ML classification model-F-A, we predicted 60 novel 2DFM materials as shown in Table S6. We input these 60 2DFM materials into model-R for regression prediction of the magnetic moment. After the regression calculations, we performed screening to obtain 13 2DFM materials with magnetic moments > 7 μ_B, as shown in Table 3. Thus, starting from an initial dataset of 60 ferromagnetic candidates, we obtained a small dataset of 13 samples that were calculated to be stable and to have net magnetic moments of > 7 μ_B. We emphasize that our goal was achieved without high-throughput DFT calculations. Here, we re-examine the anomalous point appearing in the regression model, i.e., the magnetic moment prediction of Fe_4S_8, as shown in Fig. 9(a).

Table 3 | The 13 two-dimensional materials with a magnetic moment greater than 7 μ_B are predicted by model-R.

Formula	Magnetic Moment (μ_B)
Mn_3S_4	7.661
Mn_3Se_4	7.737
$GaMnBr_5Cl$	7.813
Mn_2NS_2	7.371
In_2MnS_4	7.677
Mn_2Cl_2Se	7.447
Fe_3GeSe_2	7.308
$Mn_4N_3S_2$	12.431
$Mn_2I_2S_2$	7.603
Mn_2I_2Se	7.599
Al_2MnTe_4	7.809
Os_2Cl_8	8.435
Mn_2Te_4	7.482

An anomalous point also occurs in the regression model with a feature containing the magnetic moment of a single atom (M-single atom), such as the yellow dot in the rectangular box in Fig. S3. In the C2DB database, Fe_4S_8 are labeled as FM state with a net magnetic moment of 3.759 μ_B, which is clearly the magnetic moment of a single Fe atom. This is consistent with the GGA+*U* calculations. The unit cell used in our DFT calculations contained four Fe atoms in, the calculated net magnetic moment was 15.253 μ_B, with an average magnetic moment of 3.813 μ_B for each Fe atom. However, the crystal symmetry of Fe_4S_8 is relatively low, and the crystal field is not a conventional octahedral, tetrahedral, triangular prism. From a purely structural perspective, the nearest- neighbor Fe-Fe interaction is a direct exchange interaction. According to the interpretability analysis of our regression model, a shorter nearest neighbor direct exchange has a more significant impact on the net magnetic moment, resulting in a smaller net magnetic moment per unit cell. This is why anomalous prediction points appear in our ML regression models. In addition, the dynamic stability of Fe_4S_8 is relatively low, and further experimental confirmation of its magnetic properties is required.

MATERIALS

DOI:10.1016/j.chip.20xx.1000xx

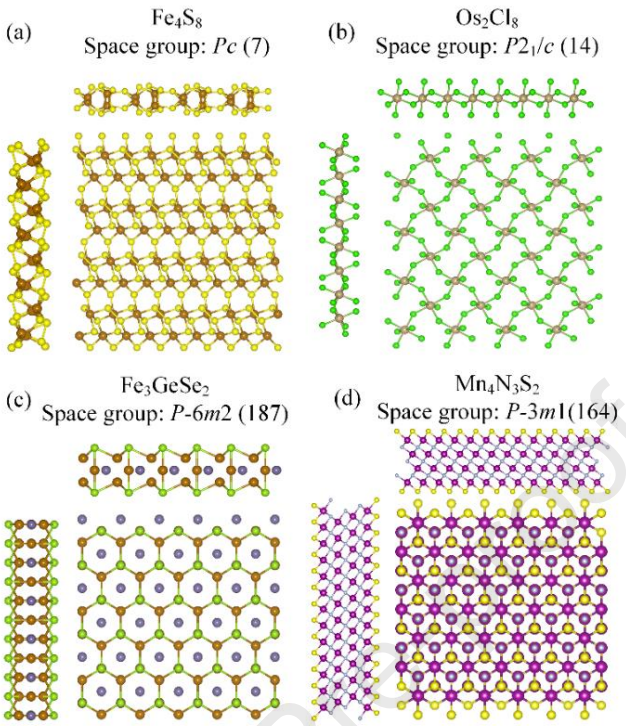

Fig. 9 | The top and side view of structure of 2D ferromagnetic materials generative by ML regression, (a) Fe_4S_8, (b) Os_2Cl_8, (c) Fe_3GeSe_2, (d) $Mn_4N_3S_2$.

In our predicted set, most of the 2D materials with large net magnetic moments contained the Mn atoms. Os_2Cl_8 and Fe_3GeSe_2 are exceptions; their structures are shown in Figs. 9(b) and (c), respectively. Os_2Cl_8 was classified as a magnetic state with a magnetic moment of 7.668 μ_B in the C2DB dataset, which was smaller than our predicted value of 8.435 μ_B. Os_2Cl_8 has high thermodynamic and dynamic stability, which was also reported for C2DB dataset. In addition, there are no relevant reports on Os_2Cl_8. Fe_3GeSe_2 has the same structural prototype as Fe_3GeTe_2, which was reported to be a ferromagnetic monolayer by Li et al.[58] The net magnetic moment of Fe_3GeSe_2 is 6.429 μ_B, which is smaller than our predicted value of 7.308 μ_B. We also found that the S-functionalized Mn-based MXene $Mn_4N_3S_2$ has the largest net magnetic moment 12.431 μ_B among the sub-dataset, which is larger than that of C2DB (10.776 μ_B). Both Fe_3GeTe_2 and $Mn_4N_3S_2$ exhibit high thermodynamic and dynamic stabilities. To verify the accuracy of the regression model, the magnetic and electronic properties of the three compounds were calculated using DFT. As shown in Fig. 10, the projected density of states (DOS) and spin density of Os_2Cl_8, Fe_3GeSe_2, and $Mn_4N_3S_2$ were obtained by the GGA+*U* approach. The band-gap of Os_2Cl_8 is 1.54 eV, which is larger than that of C2DB (0.21 eV). The net magnetic moment of the Os_2Cl_8 unit cell is 8.075 μ_B. The predicted magnetic moment (8.435 μ_B) is closer to the calculated value based on DFT than the value in the C2DB database. The magnetic moment mainly originates from Os ions, and a small portion originates from Cl ions. For Fe_3GeSe_2 and $Mn_4N_3S_2$, the DOS indicates metallic characteristic; the

MATERIALS DOI:10.1016/j.chip.20xx.1000xx

calculated magnetic moments are 7.933 μ_B and 12.844 μ_B, respectively, which agree well with the predicted ones, where the magnetic moment mainly originates from the unpaired electrons in the 3*d* orbitals of TMs Fe and Mn.

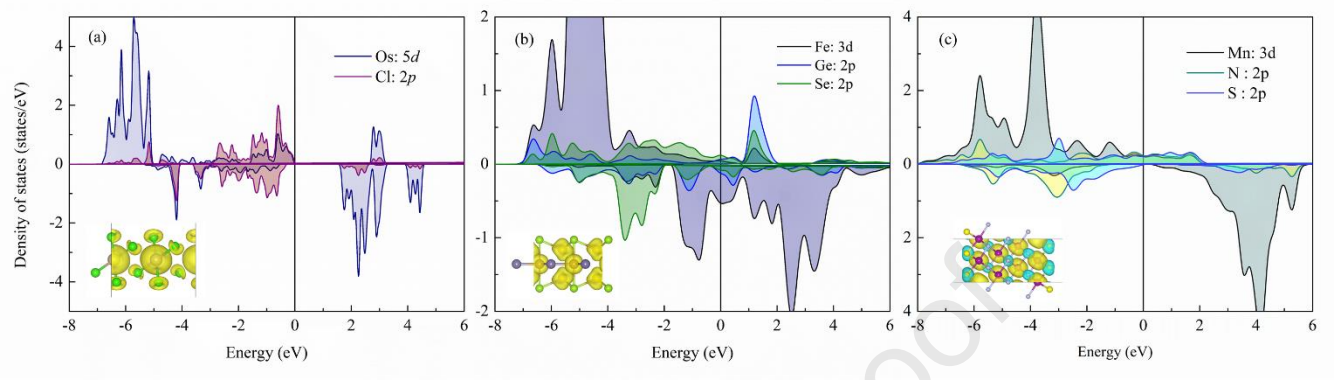

Fig. 10 | The projected density of states (PDOS) for: (a) Os_2Cl_8, (b) Fe_3GeSe_2, (c) $Mn_4N_3S_2$, monolayer. Inset: spin density.

The high-throughput DFT calculations for the 615 candidates took approximately 57600 core-hours on an HPC cluster running on Intel Xeon Gold 5218 processors. The training and screening of the ML classification and regression models took approximately 560 core-hours on an Intel(R) Xeon(R) Platinum 8259CL. The computational time was reduced by more than one order of magnitude during this process; thus, we used ML to accelerate the discovery of new 2DFM materials.

CONCLUSIONS

In this work, based on the two-dimensional material database C2DB and 2DMP, we have established machine learning models for magnetic/non-magnetic, AFM/FM classification. Combining high-throughput DFT calculations, we trained a regression model for the net magnetic moment of 2D materials. The GBDT regression model shows the best performance with R^2 = 0.945, *RMSE* = 0.649, *MAE* = 0.430 μ_B, respectively. Through the analysis of SHAP values, we have discovered that the interactions between nearest-neighbor and next-nearest-neighbor atoms play a significant role in determining the magnetic properties of 2DFM. If the interactions between nearest-neighbor and next-nearest-neighbor atoms are stronger, it implies a more pronounced magnetic coupling effect between the atoms, leading to mutual enhancement of magnetic moments. It is unexpectedly found that Cr_2NF_2 is a potential AFM/ferroelectric 2D multiferroic material. More importantly, sixty novel 2D ferromagnetic candidates are predicted, among them, 13 candidates have magnetic moments greater than 7 μ_B. Os_2Cl_8, Fe_3GeSe_2, and $Mn_4N_3S_2$ are predicted to be novel 2DFM semiconductor, half-metal, and metal, respectively. Our ML approach can accelerate the prediction of 2D ferromagnetic materials with strong magnetization, and save more than an order of magnitude in computing time.

MATERIALS DOI:10.1016/j.chip.20xx.1000xx

DATASETS AND METHODS

Datasets

C2DB and 2DMP were used as the primary sources of the dataset. It should be noted that C2DB includes 4035 entries up to 2021; however, up to 2023.03, the C2DB includes 15733 entries. The 2DMP dataset contains 6351 data in total. According to the C2DB report, there were 1617 2D materials with thermodynamic and dynamic stability in 4035 samples. Among the 1617 candidates, 1292 were non-magnetic, and 325 were magnetic. To avoid as imbalance between the magnetic and non-magnetic datasets, we randomly selected 800 magnetic 2D materials with thermodynamic and dynamic stability in the 2DMP dataset. Thus, we constructed a dataset of 2417 samples, of which 1292 were non-magnetic and 1125 were magnetic. We labeled this dataset as data-N-M and used it to train the magnetic/nonmagnetic classification model. We also found 615 magnetic samples with magnetic moments of > 1 μ_B in C2DB with 4035 entries. However, they did not include antiferromagnetic 2D samples. Even, a large database of 15733 2D materials contained only 17 samples marked as AFM. In this context, high-through-put DFT calculations for 615 FM samples were performed using our workflow. The retrieved datasets were used to train the FM and AFM classification models. We labeled this dataset as data-F-A. An accurate FM dataset with 383 samples calculated using DFT+*U* was used to train the regression model of the magnetic moment, and we defined the FM dataset as data-R. Compared with previous studies, the datasets used contained a more extensive and precise variety of 2DFM materials.

Feature engineering

The properties of a functional material can be determined either from experimental measurements or through in simulations, via calculations using an *ab-initio* approach. ML eliminates the need for expensive programs by predicting the target properties of novel 2D materials using suitable feature descriptors based on prior data. The selection of a suitable set of feature descriptors that determine the target property is of vital importance in all ML computations. Because all the properties of a material are ultimately functions of its structure, composition and elemental properties, we adopt feature descriptors that encode this information.[31] For the magnetic-nonmagnetic classification model, the feature set includes descriptors of two types: the first one is the Materials Agnostic Platform for Informatics and Exploration (MAGPIE),[32] which was proposed by Ward et al. and is used to obtain the elemental property labeled as *EP*. The second feature is the composition, which includes the number of space groups. For the FM/AFM classification model, we expanded the feature-descriptor space by including the number of *d* orbital electrons on the TM atoms (n_d) which are strongly correlated for magnetization, and the atom centered symmetry function (ACSF), which depends on the local coordination environment around a specific atom.[33] In addition, the ionic radius,

electronegativity, and dipole polarization of the TM and nearest-neighbor coordination atom were taken from the Python Mendeleev package,[34] which are largely responsible for FM/AFM classification. For the regression model of magnetization, we added Smooth Overlap of Atomic Positions (SOAP) features and sine Coulomb matrix features associated with the structure, which were labeled as *STRUCT*.[35] We considered the unpaired d orbital electrons of TM as an important feature descriptor.

High-throughput DFT calculation

Our high-throughput first-principles calculations for data-F-A were performed in the framework of DFT as implemented in the Vienna *ab-initio* simulation package code.[36,37] The generalized gradient approximation (GGA)[38] with DFT–D3 was used to describe the exchange correlation, which was a semiempirical dispersion–correction method to correct the van der Waals (vdw) interactions.[39] GGA+*U* correction was applied to strongly correlate the TM *d* orbitals.[40] We determined the *U* value through linear response theory, and thus made sure our qualitative calculated results are reliable. The corresponding *U* values of each TM are presented in Table SI. The plane-wave energy cutoff was set to 500 eV. The Brillouin zone integration was sampled with a Monkhorst–Pack[41] mesh of 8 × 8 × 1. All the structure parameters were sequentially relaxed such that the Hellmann–Feynman forces were < 0.01 eV/Å, and the total energy changes converged to < 10^{-5} eV. The conjugate gradient algorithm[42] was used to optimize the structure. A vacuum distance of > 15 Å was set between adjacent slabs to eliminate spurious interactions. Structure and spin density visualization and analysis were performed using the VESTA code.[43]

REFERENCE

1. Klein, D. R. et al. Probing magnetism in 2D van der waals crystalline insulators via electron tunneling. *Science* **360**, 1218–1222 (2018). https://doi.org/10.1126/science.aar3617.
2. Feng, Y. P. et al. Prospects of spintronics based on 2D materials. *Wiley Interdiscip. Rev. Comput. Mol. Sci.* **7**, e1313 (2017). https://doi.org/10.1002/wcms.1313.
3. Farooq, M. U. & Hong, J. Switchable valley splitting by external electric field effect in graphene/CrI_3 heterostructures. *npj 2D Mater. Appl*. **3**, 3 (2019). https://doi.org/10.1038/s41699-019-0086-6
4. Soumyanarayanan, A., Reyren, N., Fert, A. & Panagopoulos, C. Emergent phenomena induced by spin-orbit coupling at surfaces and interfaces. *Nature* **539**, 509–517 (2016). https://doi.org/10.1038/nature19820
5. Mermin, N. D. & Wagner, H. Absence of ferromagnetism or antiferromagnetism in one- or two-dimensional isotropic Heisenberg models. *Phys. Rev. Lett*. **17**, 1133–1136 (1966). https://doi.org/10.1103/PhysRevLett.17.1133
6. Huang, B. et al. Layer-dependent ferromagnetism in a van der Waals crystal down to the monolayer limit. *Nature* **546**, 270–273 (2017) https://doi.org/10.1038/nature22391
7. Gong, C. et al. Discovery of intrinsic ferromagnetism in two-dimensional van der Waals crystals. *Nature* **546**, 265 (2017). https://doi.org/10.1038/nature22060
8. O'Hara, D. J. et al. Room temperature intrinsic ferromagnetism in epitaxial manganese selenide films in the monolayer limit. *Nano Lett*. **18**, 3125–3131 (2018). https://doi.org/10.1021/acs.nanolett.8b00683
9. Deng, Y. et al. Gate-tunable room-temperature ferromagnetism in two dimensional Fe_3GeTe_2. *Nature* **563**, 94–99 (2018).

https://doi.org/10.1038/s41586-018-0626-9

10. A. K. Nair, S. Rani, M. V. Kamalakar, and S. J. Ray. Bi-stimuli assisted engineering and control of magnetic phase in monolayer CrOCl. *Phys. Chem. Chem. Phys*. **22**, 12806 (2020). https://doi.org/10.1039/D0CP01204A
11. S. Kar, A. K. Nair, and S. J. Ray. Supreme enhancement of ferromagnetism in a spontaneous-symmetry-broken 2D nanomagnet. *J. Phys. D: Appl. Phys*. **54**, 105001 (2021). https://doi.org/10.1088/1361-6463/abc64c
12. A. K. Nair and S. J. Ray. Electronic phase-crossover and room temperature ferromagnetism in a two-dimensional (2D) spin lattice. *RSC Adv*. **11**, 946-952 (2021). https://doi.org/10.1039/D0RA09726H
13. S. Guha, A. Kabiraj, and S. Mahapatra. High-throughput design of functional-engineered MXene transistors with low-resistive contacts. *npj Computational Materials*. **8**, 202 (2022). https://doi.org/10.1038/s41524-022-00885-6
14. M. N. Gjerding, A. Taghizadeh, A. Rasmussen, S. Ali, F. Bertoldo, T. Deilmann, U. P. Holguin, N. R. Knøsgaard, M. Kruse, A. H. Larsen, S. Manti, T. G. Pedersen, T. Skovhus, M. K. Svendsen, J. J. Mortensen, T. Olsen, K. S. Thygesen. Recent Progress of the Computational 2D Materials Database (C2DB). *2D Materials* **8**, 044002 (2021). https://doi.org/10.1088/2053-1583/ac1059
15. Zhou, J., Shen, L., Costa, M.D. et al., 2DMatPedia, an open computational database of two-dimensional materials from top-down and bottom-up approaches. *Sci Data* **6**, 86 (2019). https://doi.org/10.1038/s41597-019-0097-3
16. N. Mounet, M. Gibertini, P. Schwaller, D. Campi, A. Merkys, A. Marrazzo, T. Sohier, I. E. Castelli, A. Cepellotti, G. Pizzi & N. Marzari, Two-dimensional materials from high-throughput computational exfoliation of experimentally known compounds, *Nat. Nanotech*. **13**, 246–252 (2018). https://doi.org/10.1038/s41565-017-0035-5
17. Li, J., Lim, K., Yang, H., Ren, Z., Raghavan, S., Chen, P.Y., Buonassisi, T., and Wang, X. AI applications through the whole life cycle of material discovery. *Matter* **3**, 393–432 (2020) https://doi.org/10.1016/j.matt.2020.06.011
18. Zunger, A. Inverse design in search of materials with target functionalities. *Nat. Rev. Chem*. **2**, 0121 (2018). https://doi.org/10.1038/s41570-018-0121
19. Severson, K.A., Attia, P.M., Jin, N. et al. Data–driven prediction of battery cycle life before capacity degradation. *Nat Energy* **4**, 383–391 (2019). https://doi.org/10.1038/s41560-019-0356-8
20. Raccuglia, P., Elbert, K., Adler, P. et al. Machine-learning-assisted materials discovery using failed experiments. *Nature* **533**, 73–76 (2016). https://doi.org/10.1038/nature17439
21. Taniike, T., Takahashi, K. The value of negative results in data-driven catalysis research. *Nat Catal* **6**, 108–111 (2023). https://doi.org/10.1038/s41929-023-00920-9
22. Isayev, O., Oses, C., Toher, C. et al. Universal fragment descriptors for predicting properties of inorganic crystals. *Nat Commun* **8**, 15679 (2017). https://doi.org/10.1038/ncomms15679
23. C. Chen, W. Ye, Y. Zuo, C. Zheng, S. P. Ong, Graph Networks as a Universal Machine Learning Framework for Molecules and Crystals. *Chem. Mater* **31**, 3564 (2019). https://doi.org/10.1021/acs.chemmater.9b01294
24. T. Xie, J. C. Grossman, Crystal Graph Convolutional Neural Networks for an Accurate and Interpretable Prediction of Material Properties. *Phys. Rev. Lett*. **120**, 145301 (2018). https://doi.org/10.1103/PhysRevLett.120.145301
25. Zhen-Xiong Shen, Chuanxun Su and Lixin He. High-throughput computation and structure prototype analysis for two-dimensional ferromagnetic materials. *npj Computational Materials* **8**.132 (2022). https://doi.org/10.1038/s41524-022-00813-8
26. Shuaihua Lu, Qionghua Zhou, Yilv Guo, and Jinlan Wang. On-the-fly interpretable machine learning for rapid discovery of two-dimensional ferromagnets with high Curie temperature. *Chem* **8**, 769–783. https://doi.org/10.1016/j.chempr.2021.11.009
27. Carlos Mera Acosta, Elton Ogoshi, Jose Antonio Souza, and Gustavo M. Dalpian. Machine Learning Study o f the Magnetic Ordering in 2D Materials. *ACS Appl. Mater. Interfaces*. **14**, 9418−9432 (2022). https://doi.org/

10.1021/acsami.1c21558

28. Arnab Kabiraj, Mayank Kumar and Santanu Mahapatra. High-throughput discovery of high Curie point two-dimensional ferromagnetic materials. *npj Computational Materials.* **6**. 35. (2020) https://doi.org/10.1038/s41524-020-0300-2
29. Shuaihua Lu, Qionghua Zhou, Yilv Guo, Yehui Zhang, Yilei Wu, and Jinlan Wang. Coupling a Crystal Grap h Multilayer Descriptor to Active Learning for Rapid Discovery of 2D Ferromagnetic Semiconductors/Half-Me tals/Metals. *Adv.Mater*. **32**, 2002658 (2020). https://doi.org/10.1002/adma.202002658
30. Arijit Dutta, and Prasenjit Sen. Machine learning assisted hierarchical filtering: a strategy for designing magnets with large moment and anisotropy energy. *J. Mater. Chem. C*, **10**, 3404 (2022). https://doi.org/10.1039/d1tc03776e
31. Li, S, Liu, Y, Chen, D, Jiang, Y, Nie, Z, Pan, F. Encoding the atomic structure for machine learning in materials science. *WIREs Comput Mol Sci*. **12**. e1558 (2022). https://doi.org/10.1039/d1tc03776e
32. Ward, L., Agrawal, A., Choudhary, A. & Wolverton, C. A general-purpose machine learning framework for predicting properties of inorganic materials. *NPJ Comput. Mater*. **2**, 1–7 (2016). https://doi.org/10.1038/npjcompumats.2016.28
33. L. Himanen, M. O. J. Jäger, E. V. Morooka, F. Federici Canova, Y. S. Ranawat, D. Z. Gao, P. Rinke and A. S. Foster, DScribe: Library of descriptors for machine learning in materials science. *Comput. Phys. Commun*. **247**, 106949 (2020). https://doi.org/10.1016/j.cpc.2019.106949
34. L. M. Mentel, Mendeleev – A Python resource for properties of chemical elements, ions and isotopes., (2014). Available at: https://github.com/lmmentel/mendeleev.
35. Albert P. Bartók, Risi Kondor, and Gábor Csányi. On representing chemical environments. *Phys. Rev. B* **87**, 184115 (2013). https://doi.org/10.1103/PhysRevB.96.019902
36. Kresse. G, Hafner. J. Ab initio molecular dynamics for liquid metals. *Phys. Rev. B* **47**, 558 (1993). https://doi.org/10.1103/PhysRevB.47.558
37. Kresse. G. and Furthmüller. J. Efficient iterative schemes for ab initio total-energy calculations using a plane-wave basis set, *Phys. Rev. B*. **54**, 11169 (1996). https://doi.org/10.1103/PhysRevB.54.11169
38. P. E. Blöchl, Projector augmented-wave method. *Phys. Rev. B*. **50**, 17953 (1994). https://doi.org/10.1103/PhysRevB.50.17953
39. Tkatchenko, A.; Scheffler, M. Accurate Molecular Van Der Waals Interactions from Ground-State Electron Density and Free Atom Reference Data. *Phys. Rev. Lett*. **102**, 073005 (2009). https://doi.org/10.1103/PhysRevLett.102.073005
40. S. L. Dudarev, and A. P. Sutton, et al. Electron-energy-loss spectra and the structural stability of nickel oxid e: An LSDA+*U* study. *Phys. Rev. B*, **57**, 1505 (1998). https://doi.org/10.1103/PhysRevB.57.1505
41. H. J. Monkhorst and J. D. Pack, Special points for Brillouin-zone integrations. *Phys. Rev. B* **13**, 5188 (1976). https://doi.org/10.1103/PhysRevB.13.5188
42. P. Pulay, Convergence acceleration of iterative sequences. the case of SCF iteration. *Chem. Phys. Lett*. **73**, 393-398 (1980). https://doi.org/10.1016/0009-2614(80)80396-4
43. K. Momma and F. Izumi, VESTA 3 for three-dimensional visualization of crystal, volumetric and morphology data, J. Appl. Cryst, 2011, 44, 1272-1276 https://doi.org/10.1107/S0021889811038970.
44. Pedregosa F, et al. *J. Mach. Learn. Res*. **12** 2825 (2011).
45. Tiwari, S, Van de Put, ML, Soree, B, Vandenberghe, WG. Critical behavior of the ferromagnets CrI_3, $CrBr_3$, and $CrGeTe_3$ and the antiferromagnet $FeCl_2$: A detailed first-principles study, *Phys. Rev. B.* **13**, 5188 (1976). https://doi.org/10.1103/PhysRevB.103.014432
46. Daniele T, Kristian. S. T, and Thomas. O. High throughput computational screening for 2D ferromagnetic materials: the critical role of anisotropy and local correlations. *2D Mater*. **6**, 045018. (2019). https://doi.org/10.1088/2053-1583/ab2c43
47. S. Lebègue, T. Björkman, M. Klintenberg, R. M. Nieminen, and O. Eriksson. Two-Dimensional Materials from Data

Filtering and Ab Initio Calculations. *Phys. Rev. X* **3**, 031002 (2013). https://doi.org/10.1103/PhysRevX.3.031002

48. C. Xin, B. Q. Song, Y. H. Yin, A. Wang, Z. X. Sun, G. Y. Jin, and F. Pan. Charge Disproportionation Induced Multiferroics and Electric Field Control of Magnetism in 2D MXene Mo_2NCl_2. *Nanoscale*. xx xx-xx. (2023)
49. Xin, C, Fan, Z, Sun, Z. X. Pan, F. and Sui, Y. et al. Asymmetric Janus functionalization induced magnetization and switchable out-of-plane polarization in 2D MXene Mo_2CXX', *Phys. Chem. Chem. Phys*. **25**, 8676 (2023). https://doi.org/10.1039/d2cp05668b
50. Huang, B., Clark, G., Navarro-Moratalla, E. et al. Layer-dependent ferromagnetism in a van der Waals crystaldown to the mon olayer limit. *Nature* **546**, 270–273 (2017). https://doi.org/10.1038/nature22391
51. Gong, C. et al. Discovery of intrinsic ferromagnetism in two-dimensional van der Waals crystals. *Nature* **546**, 265–269 (2017). https://doi.org/10.1038/nature22060
52. Itsuki. M, Yuzuru. T, and Keisuke. T. Accelerating the discovery of hidden two-dimensional magnets using machine learning and first principle calculations. *J. Phys.: Condens. Matter* **30**. 06LT01 (2018). https://doi.org/10.1088/1361-648X/aaa471
53. Teng. L, Nuno. M. F, Zhang. Y. X, Oliver. G, and Zhang. H. B. An accelerating approach of designing ferromagnetic materials via machine learning modeling of magnetic ground state and Curie temperature. *Mater. Res. Lett*. **9**, (4), 169–174 (2021). https://doi.org/10.1080/21663831.2020.1863876
54. Ward L, Dunn A, Faghaninia A, Zimmermann. N. E. R, Bajaj S, Wang. Q, Montoya J, Chen. J. M, Bystrom. K, Dylla. M, Chard K, Asta M, Persson K A, Snyder G J, Foster I, Jain A. Matminer: An open source toolkit for materials data mining. *Comput. Mater. Sci*. **152**. 60 (2018). https://doi.org/10.1016/j.commatsci.2018.05.018
55. Zheng. F. W, Magnetic Skyrmion Lattices in a Novel 2D-Twisted Bilayer Magnet. *Adv. Funct. Mater*. **33**, 2206923 (2023). https://doi.org/10.1002/adfm.202206923
56. Lundberg, S.M, et al. From local explanations to global understanding with explainable AI for trees. *Nat. Mach. Intell*. **2**, 56–67 (2020). https://doi.org/10.1038/s42256-019-0138-9
57. Shucheng Xing, Jian Zhou, Xuanguang Zhang, Stephen Elliott, Zhimei Sun, Theory, properties and engineering of 2D magnetic materials. *Progress in Materials Science*. **132**. 101036 (2023). https://doi.org/10.1016/j.pmatsci.2022.101036
58. Li. Q, and Qiu. Z. Q et al. Patterning-Induced Ferromagnetism of Fe_3GeTe_2 van der Waals Materials beyond Room Temperature. *Nano Lett*. **18**, 9, 5974–5980 (2018). https://doi.org/10.1021/acs.nanolett.8b02806

MISCELLANEA

Supplementary material (delete if not applicable) Supplementary material associated with this article can be found, in the online version, at doi:xxx.

Acknowledgments (or Funding) This work was supported by the National Natural Science Foundation of China (No. U19A2077), and Soft Science Research Project of Guangdong Province (No. 2017B030301013). We thank the High Performances Computing Center of School of Advanced Materials, Peking University Shenzhen Graduate School for calculation resource.

Declaration of Competing Interest The authors declare no competing interests.

Declaration of Competing Interest

The authors declare no competing interests.